

Reducing RES Droughts through the integration of wind and PV

Boris Morin^{a,*}, Aina Maimó Far^a, Damian Flynn^b, Conor Sweeney^a

*^aSchool of Mathematics and Statistics, University College Dublin, Belfield, Dublin
4, Dublin, D04 V1W8, Ireland*

*^bSchool of Electrical and Electronic Engineering, University College Dublin, Belfield,
Dublin 4, Dublin, D04 V1W8, Ireland*

*Corresponding author

Email addresses: `boris.morin@ucdconnect.ie` (Boris Morin),
`aina.maimofar@ucd.ie` (Aina Maimó Far), `damian.flynn@ucd.ie` (Damian Flynn),
`conor.sweeney@ucd.ie` (Conor Sweeney)

Abstract

Increasing the share of electricity produced from renewable energy sources (RES), combined with RES dependence on weather, poses a critical challenge for energy systems. This study investigates the importance of the balance between wind and photovoltaic (PV) capacity on periods of low renewable generation, known as RES droughts. Three different RES models are used to estimate the capacity factors for different scenarios of installed capacities for wind and PV power. The skill of the RES models is quantified by comparing capacity factor time series to observed hourly data and by assessing their representation of observed RES droughts. The RES models are used to generate a 45-year hourly time series of RES capacity factor, enabling analysis of the frequency, duration and return periods of RES droughts at a climatological scale. Results show the importance of using an accurate, validated RES model for RES drought risk assessment. The addition of PV capacity to a wind-dominated system results in a significant reduction in the frequency and duration of RES droughts, while also reducing extremes and seasonal drought patterns. These findings underscore the importance of diversification in RES capacity to enhance energy security and resilience.

Keywords: RES Drought, Wind Power, Solar PV Power, Renewable Energy Sources, Return Periods

1. Introduction

The EU aims to generate at least 69% of its electricity from renewable energy sources (RES) by 2030, up from 41% in 2022 [1]. While this transition is essential for reducing greenhouse gas emissions, it also highlights the challenge of managing the variability of weather-dependent energy sources such as wind and photovoltaic (PV) power. This challenge is compounded by the increasing electrification of energy sectors, which places greater demand on the power system and makes it more sensitive to meteorological conditions [2, 3, 4]. Periods of low renewable generation, known as *Dunkelflaute* or RES droughts, pose significant risks to system adequacy and energy security, emphasising the need for a resilient energy system to meet both growing electricity demand and decarbonisation targets.

This study focuses on Ireland, a region with a strong reliance on wind power, which has ambitious targets for PV power expansion. This case study

15 provides valuable insights into the potential benefits of diversifying the re-
16 newable energy mix on RES droughts. The performance of different RES
17 models are compared, and a 45-year time series of RES generation is pro-
18 duced. The results highlight the role of increased PV capacity in reducing
19 RES drought risks, offering insights for policymakers and energy planners.

20 For this study, a RES drought event is defined as occurring when the
21 average capacity factor (CF) remains below a fixed threshold for a given du-
22 ration, following the methodology used in other research [5, 6, 7, 8]. Alterna-
23 tive methods exist for defining RES droughts. One approach uses relative CF
24 thresholds that change over the year to account for seasonal variations in re-
25 newable energy generation [9, 10, 11, 12, 13]. Another common method relies
26 on percentile-based thresholds, where drought events are defined by identi-
27 fying periods of unusually low generation relative to historical production
28 levels, typically based on the lowest production percentiles [12, 14]. Addi-
29 tionally, some studies combine these definitions with metrics that incorporate
30 the demand side of energy consumption, analysing the balance between sup-
31 ply and demand during drought periods [9, 10, 12, 14]. In this paper, the
32 focus is exclusively on energy generation, and a fixed threshold approach to
33 define RES droughts is used, which facilitates consistent inter-comparison
34 between scenarios with different installed wind and PV capacities.

35 RES droughts are identified using onshore wind and PV CF time series.
36 In this study, three different datasets are used, all of which are driven by
37 ERA5 data [15]. Two of the datasets are part of C3S Energy (C3S-E), an
38 energy-based operational dataset produced by the EU Copernicus Climate
39 Change Service [16, 17]. One of the C3S-E datasets provides CF time series
40 aggregated at the national scale, while the other provides the CF time series
41 at each grid point, at the ERA5 resolution of 0.25° . The third dataset was
42 generated using the Atlite model [18], which converts the ERA5 atmospheric
43 data to a generation time series using specified wind turbine and PV panel
44 models. Atlite is an open-source tool developed by PyPSA [18] and is widely
45 used for estimating wind and PV generation [7, 19, 20, 21].

46 The datasets used in this study are detailed in section 2, which describes
47 their characteristics and relevance for evaluating RES droughts. Section 3
48 outlines the RES models used to simulate wind and PV generation and pro-
49 vides the methodology for defining and identifying RES drought events, in-
50 cluding the thresholds and metrics applied. In section 4, the models are first
51 verified against observed energy data to assess their accuracy, followed by an
52 analysis of RES drought occurrences for two scenarios with different ratios

53 of installed wind to PV capacities. Finally, section 5 offers a discussion of
54 the results in the context of energy reliability and future planning, followed
55 by the main conclusions and recommendations for further research.

56 **2. Data**

57 This study uses publicly available datasets to construct and validate the
58 models for estimating the CF of wind and PV energy. The primary data
59 sources include: EirGrid and SONI, the transmission system operators (TSO)
60 for the Republic of Ireland and Northern Ireland, respectively; the ERA5
61 reanalysis dataset; and the C3S-E datasets.

62 *2.1. Wind and PV Capacity and Availability*

63 EirGrid, the TSO for the Republic of Ireland, and SONI, the Northern
64 Ireland TSO, provide detailed datasets on all wind and PV farms across the
65 island of Ireland (Republic of Ireland and Northern Ireland) from 1990 to the
66 present [22]. These datasets include information such as each farm’s installed
67 capacity, name, and connection date. To enhance the accuracy of this data,
68 the longitude and latitude for each farm were manually determined through
69 online searches. For simplicity, this data will be referred to as originating
70 from EirGrid, as all-island data was directly obtained from EirGrid, and the
71 combined regions of the Republic of Ireland and Northern Ireland will be
72 referred to as Ireland throughout the remainder of this document.

73 The spreadsheet available from the EirGrid website contains two key vari-
74 ables: generation and availability. Generation is the energy that a RES farm
75 actually contributed to the grid, which may include limitations introduced
76 by the TSO to maintain grid stability, such as constraints and curtailment.
77 Availability represents the energy that would have been generated from a
78 RES farm if no grid constraints had been applied, making it representative
79 of the weather-related response. Generation and availability values are avail-
80 able from 2014 onward for wind power and from 2018 onward for PV power,
81 although PV availability data only became present in the Republic of Ireland
82 in 2023. This study focuses on availability for all analyses.

83 *2.2. Atmospheric Variables*

84 Atlite and C3S-E datasets are driven by the ERA5 reanalysis [15], pro-
85 duced by the European Centre for Medium-Range Weather Forecasts (ECMWF).
86 This global gridded dataset provides hourly atmospheric variables from 1940

87 to the present at a horizontal resolution of 0.25° . It is widely used for esti-
88 mating PV and wind energy [7, 16, 23, 24]. Table 1 lists the ERA5 variables
89 used by Atlite and C3S-Energy.

Table 1: ERA5 variables used to calculate wind and PV generation

ERA5 name	variable
100 metre zonal and meridional wind speed	u_{100}, v_{100}
2 metre temperature	$t2m$
Surface net solar radiation	ssr
Surface solar radiation downwards	$ssrd$
Top of atmosphere incident radiation	$tisr$
Total sky direct solar radiation at surface	$fdir$

90 2.3. C3S Energy

91 The EU Copernicus Climate Change Service developed the C3S-E renew-
92 able energy dataset for Europe [16], using ERA5 atmospheric variables and
93 weather-to-energy models. This dataset provides hourly CF for wind and PV
94 energy from 1979 to the present. The data are available on the same grid as
95 the ERA5 data, which has a horizontal resolution of 0.25° . The time series
96 are also available for download at two aggregated scales: regional (NUTS 2)
97 and national.

98 The C3S-E dataset estimates wind energy using wind speeds at 100 me-
99 tres (u_{100}, v_{100}) and a standard turbine model, the Vestas V136/3450, with
100 a fixed hub height of 100 meters. This choice is based on expert advice and
101 the trend in wind turbine installation. The PV generation model used by
102 C3S-E uses two ERA5 variables: surface solar radiation downwards ($ssrd$)
103 and air temperature ($t2m$). PV generation is calculated multiple times, us-
104 ing the same model with different azimuth and tilt angles. The results are
105 aggregated based on a statistical distribution of the module angles based on
106 the geographical location [25].

107 3. Methods

108 This study uses three datasets to analyse RES droughts across the island
109 of Ireland. Data downloaded from C3S-E were used to obtain two datasets:
110 one based on national-level data (C3S-E N), and another on grid-level data
111 (C3S-E G). The third dataset was computed using the Atlite model (Atlite).

112 3.1. C3S-Energy National

113 For national-level analyses, the aggregated CF time series provided by
114 C3S-E were used at two levels: Republic of Ireland (NUTS0: IE) and North-
115 ern Ireland (NUTS2: UKN0). These are based on the assumption by C3S-E
116 that RES generation occurs at every ERA5 grid point in Ireland. We com-
117 puted a weighted average of these, based on the installed capacity of each
118 one, to represent the total CF for Ireland.

119 3.2. C3S-E Gridded

120 The gridded dataset from C3S-E was used to create CF datasets which
121 account for the location of RES farms in Ireland. A list of the RES farms in
122 Ireland was compiled, including each farm’s latitude, longitude and installed
123 capacity. Using these coordinates, the nearest grid point on the C3S-E grid
124 was identified for each farm. The CF values from the C3S-E dataset corre-
125 sponding to these grid points were retrieved. A weighted average of the CF
126 values was calculated, with the installed capacity of each farm serving as the
127 weight, to construct the CF time series for Ireland. This process resulted in
128 a time series of RES generation for each energy source (wind and PV) for
129 Ireland, which takes the location of the RES farms into account.

130 3.3. Atlite

131 Atlite transforms weather data into energy data using the gridded ERA5
132 data and the locations of existing RES farms, as described in C3S-E G.
133 ERA5 data for wind speed at 100 metres (u_{100} , v_{100}) are used to calculate
134 wind generation, while the ERA5 radiation variables (ssr , $ssrd$, $tisr$, and
135 $fdir$) and air temperature ($t2m$) are used to calculate PV generation. A
136 key distinction between C3S-E and Atlite lies in their representation of wind
137 turbines and PV panels. This study identifies the most appropriate wind
138 turbine power curve to use from the 121 power curves made available by
139 Renewables.ninja [26]. The selection of a specific wind turbine and PV panel
140 characteristics is further discussed and explained in section 4.1.

141 3.4. Energy Scenarios

142 In addition to analysing wind and PV generation separately, a combined
143 CF was computed for each model by averaging wind and PV generation,
144 weighted by their installed capacities at the end of 2023 (5.9 GW for wind
145 power and 0.6 GW for PV power). This configuration is referred to as the

146 91W-9PV scenario, reflecting the distribution of 91% wind and 9% PV ca-
147 pacity. Given that PV capacity in Ireland is low in 2023, and to explore how
148 a more balanced distribution of wind and PV capacities might impact RES
149 droughts, this study also considered a second scenario, referred to as 57W-
150 43PV, where the installed PV capacity is assumed to increase to 8.6 GW,
151 while wind capacity rises to 11.45 GW. These values are based on targets
152 outlined in the roadmap published by the 2024 Climate Action Plan [27].
153 This study does not include offshore wind in the analysis. Recent reports
154 suggest that even by 2030, Ireland is unlikely to have any significant new off-
155 shore wind farms, with projected offshore capacity expected to remain near
156 zero using realistic scenarios [28].

157 New time series were generated for both the Atlite and C3S-E G PV mod-
158 els, incorporating a revised distribution of installed capacity across Ireland
159 as specified in the roadmap. For wind power, the CF time series remains un-
160 changed, as significant shifts in the location of wind farms are not expected.
161 In total, twelve CF time series were analysed in this study, six for individual
162 wind and PV CF (three models for each source) in the 91W-9PV scenario,
163 and an additional six time series that include the combined CF for 91W-9PV
164 and 57W-43PV scenarios across the different models.

165 It is important to note that the specific capacity values used in this study
166 are illustrative and are not intended to reflect precise future realities. Instead,
167 they serve to explore the impact of transitioning from a wind-dominated sys-
168 tem (91W-9PV) to a more evenly distributed system (57W-43PV). This ap-
169 proach allows for a comparative analysis between the two scenarios, assessing
170 how the balance of RES capacity affects the occurrence of RES droughts.

171 3.5. RES Drought Definition

172 In this study, a RES drought event was defined as occurring when the
173 24-hour moving average of CF remains below a fixed threshold of 0.1 for
174 a period of longer than 24 hours. The choice of this threshold is somewhat
175 arbitrary, but aligns with similar studies on low renewable energy production
176 [5, 6, 8]. By using a 24-hour moving average, fewer but longer-lasting events
177 were captured compared to using the raw CF time series, which can be more
178 sensitive to short-term fluctuations. A fixed threshold approach was chosen
179 in this study to enable consistent inter-comparison between datasets.

180 The moving average approach smooths out short-term fluctuations, so
181 that brief periods above the threshold do not interrupt an otherwise con-
182 tinuous low-CF period (Fig. 1). This means that a single hour above the

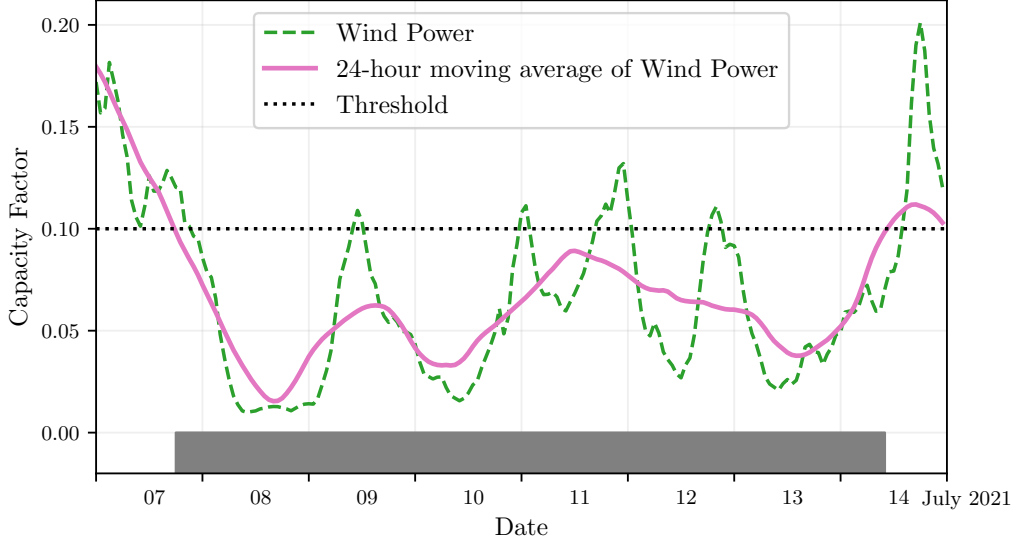


Figure 1: Wind time series of CF (green) and its 24-hour moving average (pink) from the 7th to the 15th of July 2021. The black dashed line indicates the CF threshold. The grey bar shows the period identified as a wind drought under our definition

threshold does not "break" a drought event if it is surrounded by prolonged low-generation hours. As a result, fewer but longer-lasting drought events are identified, which may better reflect real-world conditions where energy supply constraints persist over extended periods.

4. Results

4.1. Verification

The accuracy of the datasets used in this study was verified, before continuing to the analysis of RES droughts. For the verification process, time-varying values of installed capacity were used to account for changes in RES development over the verification period. This step allowed us to assess how well the datasets represent the production of renewable energy by comparing them against observed data.

4.1.1. Wind Energy

The C3S-E datasets use the Vestas V136/3450 wind turbine power curve, (Fig. 2a). The Atlite model allows the user to specify the power curve.

198 We considered the 121 power curves available for download from Renew-
 199 ables.ninja [26]. For each power curve, Renewables.ninja also provides four
 200 associated smoothed power curves. The smoothing is done using a Gaussian
 201 filter with different standard deviations that depend on the wind speed. A
 202 separate wind CF time series for Ireland was generated for each of the wind
 203 turbine power curves and smoothing levels.

204 The performance of each CF time series is then assessed based on four skill
 205 scores: correlation coefficient (CC), root mean square error (RMSE), mean
 206 bias error (MBE), and the percentage of overlap. The percentage of overlap
 207 quantifies the similarity between the observed and modelled distributions. It
 208 is a positively oriented skill score, where 100% shows full agreement between
 209 the two distributions, and 0% indicates no overlap. The histograms of hourly
 210 CF values for the most recent decade (2014-2023) are used to calculate this
 211 skill score.

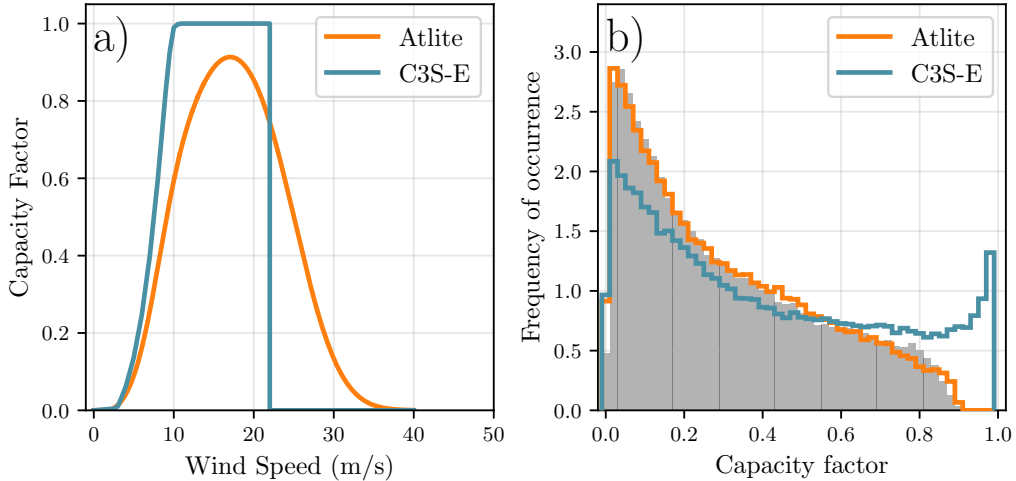


Figure 2: a) Power curves of the Enercon E112.4500 with a $0.3w$ smoothing filter used by Atlite (orange) and the Vestas V136/3450 used by C3S-E (blue) b) Histograms of wind CF for Ireland from Atlite (orange), C3S-E (blue) and Observed (shaded)

212 Based on these metrics, the most representative power curve for Ireland
 213 is the Enercon E112.4500 power curve with the $0.3w$ smoothing filter. The
 214 smoothing of the wind turbine power curve represents losses associated with
 215 each turbine, as well as losses such as wake effects between turbines, which
 216 are important when modelling wind energy on larger spatial scales. The his-
 217 togram in Fig. 2b shows that the C3S-E power curve tends to underestimate

low CF values and overestimate higher ones, whereas the smoothed Atlite power curve more closely follows the observed wind availability data. This is further supported by the percentage of overlap which is higher for Atlite (97.2%) than for C3S-E (83.2%), indicating better agreement with observed data.

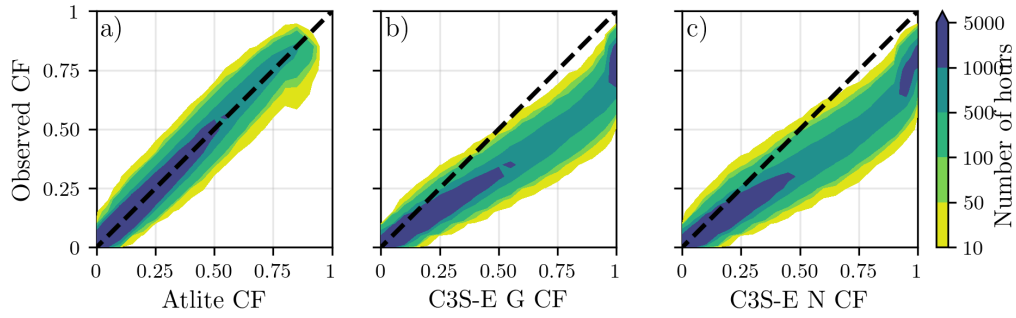


Figure 3: Wind CF density plot of the observed CF (vertical axes) and modelled (horizontal axes) CF data for the a) Atlite, b) C3S-E G and c) C3S-E N models

The effect of the difference between the power curves is also visible in Fig. 3, which shows a density plot of wind CF values. The two C3S-E datasets are shown to overestimate the observed CF, whereas the Atlite model is in good agreement with the observed data. The skill scores presented in Table 2 show that Atlite performs better than the C3S-E datasets for all of the skill scores.

	Atlite	C3S-E G	C3S-E N
CC	0.981	0.972	0.970
RMSE	0.045	0.177	0.162
MBE	-0.003	0.137	0.121

Table 2: Skill scores for wind power for the three datasets compared to observed data

Fig. 4 shows the average annual number of wind drought events during the 2014 to 2023 validation period. The figure reveals that Atlite presents the best overall agreement with the observed frequency and duration of wind drought events. This pattern is particularly evident for shorter-duration events, which are the most frequent.

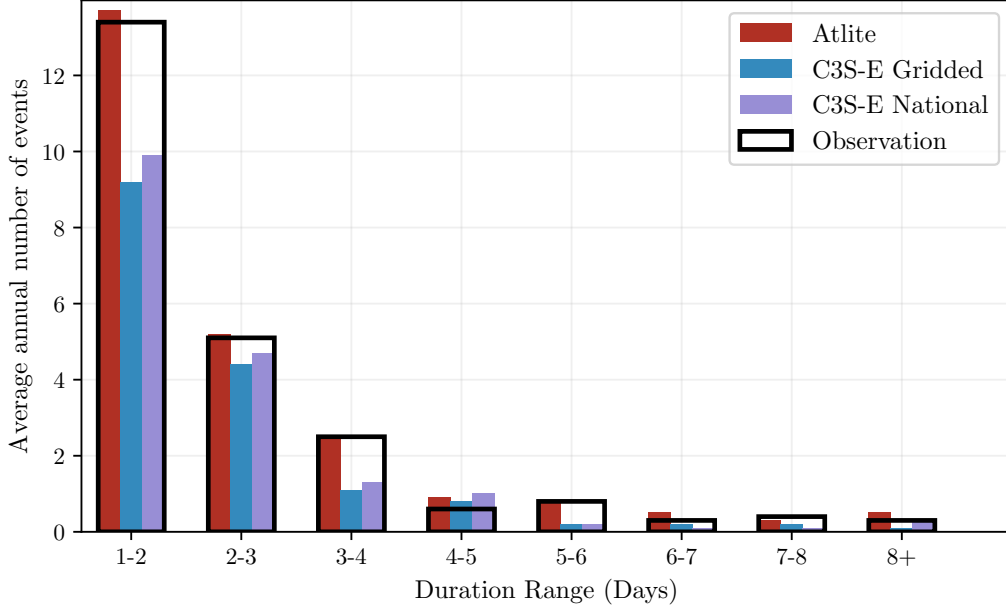


Figure 4: Average annual number of wind drought events for Atlite (red), C3S-E G (blue), C3S-E N (purple), and the observed data (black outline). The wind droughts are identified from 2014 to 2023, considering the actual capacity of the system at any given time

234 4.1.2. PV Energy

235 The Atlite model allows the user to select certain PV panel characteristics.
 236 In this study, the three PV panel types available in the Atlite model were
 237 considered (CSi, CdTe, Kaneka). Following the same methodology as in the
 238 previous section, the three available models were compared using four skill
 239 scores (CC, RMSE, MBE, and the percentage of overlap). Based on the best-
 240 performing metrics, the Breyer PV panel model was selected [29], using the
 241 Kaneka Hybrid panel option. For all PV farm locations, the azimuth angle
 242 is fixed at 180°(due south), and the optimal tilt angle option is applied.

243 The PV installed capacity available on the spreadsheets from EirGrid
 244 represents the Maximum Export Capacity (MEC) and does not accurately
 245 reflect the installed PV capacity. To enable actual PV generation potential
 246 to be modelled correctly, installed capacities were set at 1.4 times the MEC
 247 values. This scaling factor was estimated by analysing proprietary data from
 248 individual PV farms provided by EirGrid, which showed that, on average,
 249 assuming that the installed capacities of farms exceed their MEC values by

250 40% yields the best agreement with the observed availability.

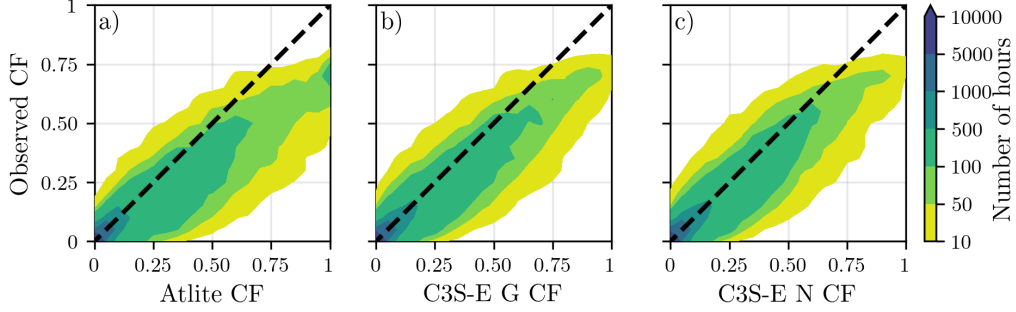


Figure 5: PV CF density plot of the observed (vertical axes) and modelled (horizontal axes) CF series for the a) Atlite, b) C3S-E G and c) C3S-E N models

251 Figure 5 shows that the three datasets have a similar tendency to overesti-
 252 mate the CF compared to the observed values, especially for high CF values.
 253 The skill scores presented in Table 3 indicate that C3S-E G performs best
 254 overall, with the lowest RMSE and a high correlation coefficient, suggesting
 255 a closer match to observed data. All models show a slight positive bias, with
 256 Atlite exhibiting a slightly lower correlation and higher RMSE.

	Atlite	C3S-E G	C3S-E N
CC	0.921	0.931	0.931
RMSE	0.119	0.090	0.113
MBE	0.046	0.027	0.021

Table 3: Skill scores for PV CF for the three datasets compared to observed data

257 Fig. 6 shows the number of PV drought events during the 2023 validation
 258 period across different duration ranges. The figure reveals partial agreement
 259 between the three datasets and the observed data, with consistent results
 260 noticed for duration ranges of 1-2, 3-4, 7-8, and 8+ days. However, dis-
 261 crepancies appear in the other ranges, where the models diverge from the
 262 observed data. The main challenge in validating PV data stems from the
 263 recent installation of a large share of Ireland’s PV capacity, with over 65%
 264 of the total PV capacity installed in 2023. This results in uncertainties in PV
 265 generation data and the actual generating capacity in the first few months
 266 after each farm is connected.

267 As the goal of this analysis is to assess the combination of wind and PV
 268 generation, the complementary nature of these energy sources mitigates the
 269 limitations in PV-only results.

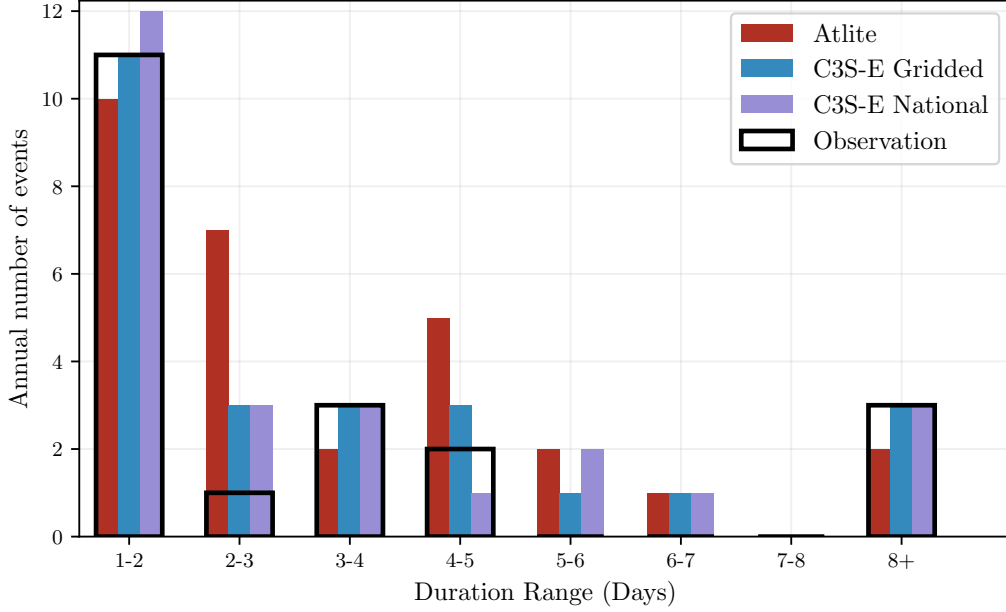


Figure 6: Number of PV drought events for Atlite (red), C3S-E G (blue), and C3S-E N (purple) and the observed data (black outline). The PV droughts are identified for 2023, considering the actual capacity of the system at any given time

270 4.2. Analysis

271 In this section, RES drought events are evaluated under two different
 272 scenarios with fixed installed capacities: the 91W-9PV scenario, with 5.9 GW
 273 of wind capacity and 0.6 GW of PV capacity; and the 57W-43PV scenario,
 274 where wind capacity comprises 11.45 GW and PV capacity increases to 8.6
 275 GW. Both scenarios were driven by 45 years of ERA5 data. Using the RES
 276 drought identification process described in Section 3.5, wind and PV droughts
 277 are first analysed separately before presenting the results for combined (wind
 278 + PV) RES droughts under both scenarios.

279 4.2.1. Annual Number of RES Droughts

280 The first part of the analysis examines the annual number of RES drought
 281 events across the three datasets. When only wind energy is considered

(Fig. 7a), the number of events decreases as the duration range increases, with very few events lasting more than seven days. In the case of only PV energy (Fig. 7b), the number of events also declines as the duration range extends from one to eight days, followed by a slight increase for longer durations. This increase occurs because Ireland, being located above the 50° parallel, experiences reduced sunlight during the winter months. From November to March, PV output often remains consistently low, leading to extended periods where generation stays below the CF threshold.

When comparing wind and PV results (Fig. 7a & b), the median, first, and third quartiles for PV are consistently higher than or equal to those for wind, across all duration ranges and datasets. This is due to the typically lower CF of PV power compared to wind power, especially in a region such as Ireland where solar potential is limited. PV generation is also zero at night and constrained by the daily solar cycle, leading to a naturally higher frequency of drought events in PV compared to wind.

Fig. 7c & d show the combination of wind and PV under the two capacity scenarios. In the 91W-9PV scenario (Fig. 7c), the identified RES droughts closely match those for wind alone, which is expected due to the dominance of installed wind capacity. In contrast, the 57W-43PV scenario (Fig. 7d) shows a clear reduction in the number of drought events across all datasets and durations, with a decrease of the total number of events of 56% for Atlite, 52% for C3S-E G, and 50% for C3S-E N. This reduction is attributed to the anti-correlation between wind and PV generation.

The median, first, and third quartiles for the Atlite dataset are consistently greater than or equal to those of the other two datasets, regardless of the duration range or type of renewable energy considered. This difference arises from the wind turbine power curve model used in the C3S-E datasets, which tends to overestimate the wind CF (Fig. 3). As a result, the overall number of RES droughts is underestimated in the C3S-E datasets compared to Atlite.

4.2.2. Return Periods of RES Drought Duration

The RES drought events identified over the 45-year period were used to calculate the return periods for different RES drought durations. A return period is the estimated average time interval between events of a specified duration or intensity (not to be confused with the frequency of their occurrence within a fixed time frame). Fig. 8 illustrates the return periods for varying RES drought durations, highlighting how often different drought lengths are

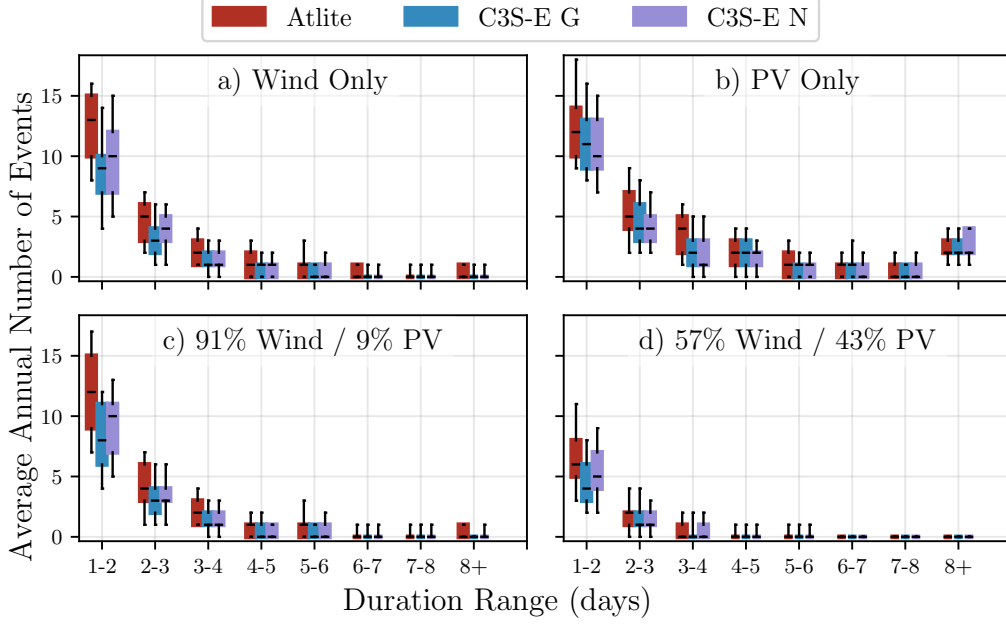


Figure 7: Average annual number of RES droughts (from 1979 to 2023) for a) Wind, b) PV, c) 91W-9PV and d) 57W-43PV for Atlite (red), C3S-E G (blue), and C3S-E N (purple). The x-axis represents duration ranges in days (lower bound included), while the y-axis indicates the annual number of events. The boxes display the first and third quartiles and the median is marked by a black line. The whiskers indicate the 5th and 95th percentiles

likely to occur across the datasets. This analysis provides insight into the frequency and likelihood of prolonged low-generation periods, which is crucial for evaluating the potential impact of RES droughts on energy reliability and security of supply.

The duration of wind droughts (Fig. 8a) increases in a log-linear fashion across the three datasets. The log-linear trend indicates a predictable relationship between drought duration and occurrence, with longer wind droughts becoming exponentially less likely as duration increases.

In the case of PV droughts (Fig. 8b), Atlite behaves differently than the two C3S-E datasets. The Atlite results show a generally log-linear increase. For C3S-E G and C3S-E N, the duration of PV droughts increases in a log-linear pattern for events lasting less than 16 days. Beyond this duration, there is a sharp rise in drought duration for events up to a one-year return period. This sudden increase again reflects the impact of extended periods

333 of low PV generation during winter in Ireland.

334 The difference between Atlite and the C3S-E results arises from differ-
335 ences in the datasets near the threshold of 0.1 CF. Atlite remains slightly
336 above the threshold more frequently during these conditions, leading to
337 shorter, more fragmented drought events. In contrast, C3S-E G and C3S-E
338 N tend to fall below the threshold in similar conditions, resulting in longer
339 continuous drought periods, especially during winter.

340 For the 91W-9PV scenario (Fig. 8c), the return periods mirror those of
341 Fig. 8a, due to the low levels of installed PV capacity. In the 57W-43PV
342 scenario (Fig. 8d), the return periods for RES droughts increase across all
343 durations. For example, the return period for a five-day drought event (shown
344 by the vertical dashed lines in Fig. 8) extends from roughly six months for
345 the 91W-9PV scenario, to four years for the 57W-43PV scenario in the Atlite
346 dataset, and from about fifteen months to around five years in the two C3S-E
347 datasets.

348 Across Fig. 8a, c, and, d, the return periods in the Atlite dataset are
349 consistently higher than those in the two C3S-E datasets. For instance, in
350 the 91W-9PV scenario (Fig. 8c), an event with a one-year return period
351 lasts six days in the Atlite dataset, compared to only five days in the C3S-E
352 datasets. This difference underscores the importance of model selection when
353 quantifying RES droughts, as each model’s assumptions and parametrisations
354 significantly influence drought duration estimates. Additionally, in all four
355 graphs, the similarity between results from the two C3S-E datasets suggests
356 that assumptions in the Atlite model—such as wind turbine power curve
357 selection and PV panel specifications—have a greater impact on RES drought
358 duration estimates than the precise geographic distribution of RES farms
359 when studying the return periods of RES droughts.

360 4.2.3. Seasonal Distribution of RES Droughts

361 The seasonality of RES droughts was analysed by comparing the percent-
362 age of hours in each month classified as part of a RES drought.

363 For wind-dominated scenarios (Fig. 9a & c), the percentage of hours that
364 are part of a drought is higher in summer than in winter. In the Atlite
365 dataset, for instance, an average of 24% of hours in summer (June-July-
366 August) are identified as wind droughts, compared to only 4% in winter
367 (December-January-February). This seasonal variation is less prominent for
368 the two C3S-E datasets compared to the Atlite one. This difference can be
369 linked to the shape of the two power curves (Fig. 2). CFs near or under the

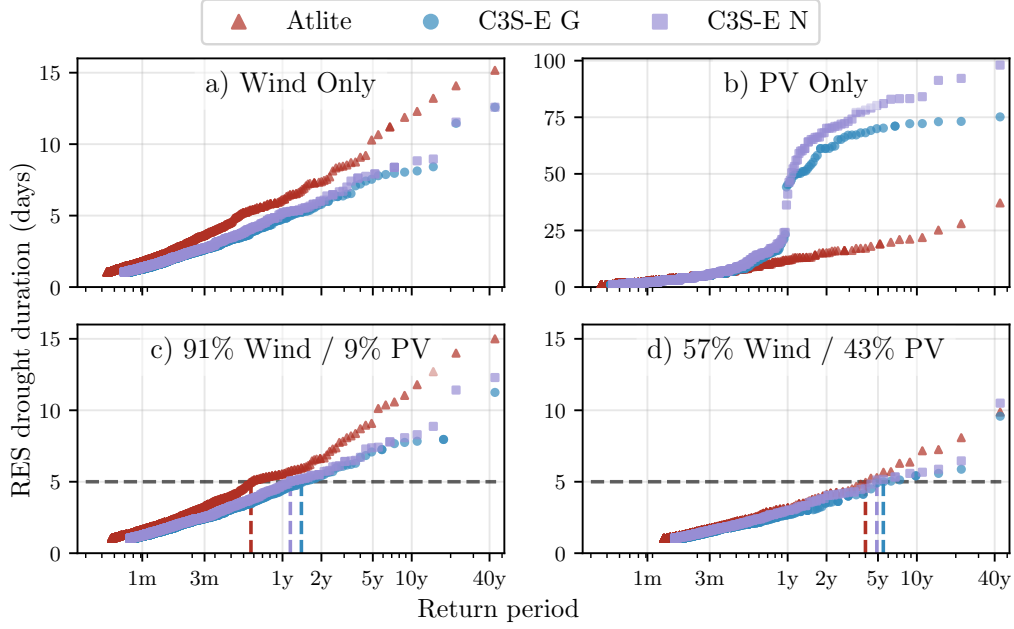


Figure 8: Return periods of the duration of RES droughts (from 1979 to 2023) for a) Wind, b) PV, c) 91W-9PV and d) 57W-43PV for Atlite (red triangle), C3S-E G (blue circle), and C3S-E N (purple square). The x-axis represents the return period time in a log-scale and the y-axis indicates the duration of RES drought associated with it. The horizontal dashed line marks the 5-day return period, with coloured vertical dashed marking its return period for each dataset

0.1 threshold occur at higher wind speeds for the Atlite power curve than for the C3S-E one. In contrast, the results for PV droughts (Fig. 9b) show a higher percentage in winter, with PV droughts occurring over 60% of the time regardless of the dataset. The Atlite results show a higher percentage of PV drought hours for wind, and a slightly lower percentage for PV, compared to the two C3S-E datasets.

The 91W-9PV scenario (Fig. 9c) shows patterns comparable to the ones for wind droughts (Fig. 9a). However, in the 91W/9PV scenario, the number of hours classified as RES droughts in summer decreases slightly compared to the wind-only scenario. This reduction can be explained by the contribution of PV generation during the summer months in the 91W-9PV scenario, even though it constitutes only 11% of total capacity. Since the number of RES drought hours for PV in summer is near zero, this small contribution has a

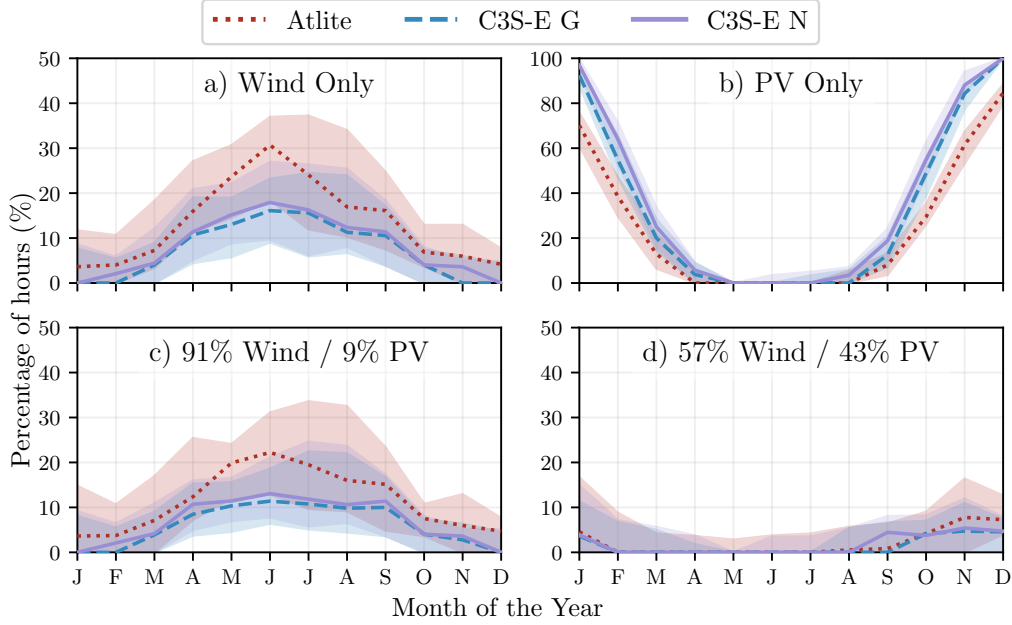


Figure 9: Percentage of hours in a month which are part of a RES drought (from 1979 to 2023) for a) Wind, b) PV, c) 91W-9PV and d) 57W-43PV for Atlite (red dotted), C3S-E G (blue dashed), and C3S-E N (purple solid). The x-axis represents the month of the year, and the y-axis indicates the percentage of hours. Lines correspond to the median values and the area between the first and third quartiles is shaded. Note the different y-axis scale for b).

noticeable impact on reducing overall drought hours. In the 57W-43PV scenario (Fig. 9d), all three datasets show a reduction in monthly RES drought frequency. Annual reductions in median RES drought frequency are observed across the datasets, dropping from 14% to 5% for Atlite, from 8% to 3% for C3S-E G, and from 9% to 4% for C3S-E N. The balanced mix of wind and PV power in this scenario reduces the seasonal signal overall and significantly decreases the percentage of RES drought hours in the summer.

5. Discussion and Conclusions

This study has investigated the ability of three RES models to represent RES droughts: Atlite, C3S-E G, and C3S-E N. One of the most evident differences is how each dataset incorporates the specific locations of RES farms. Both Atlite and C3S-E G consider the locations of wind and PV

395 farms, which one would expect to result in a more accurate representation
396 of RES generation. While this approach slightly improves PV models, our
397 analysis indicates that for wind energy, the Atlite dataset performs better
398 overall, especially in its close alignment with observed data for wind gener-
399 ation estimates. This finding suggests that, although the inclusion of RES
400 farm locations is beneficial, the accuracy of the RES model is more strongly
401 influenced by underlying model assumptions, such as selecting an appropriate
402 wind power curve.

403 Atlite shows the best alignment with observed data for wind generation.
404 Differences between the models are smaller for PV, with C3S-G performing
405 marginally better than the other two. The results show that the two C3S-E
406 datasets (C3S-E G and C3S-E N) consistently yield similar outcomes, in-
407 dicating that their methodological differences have minimal impact in this
408 case. This distinction is also evident in the analysis, where Atlite reports
409 higher return periods and a greater number of RES droughts, especially in
410 scenarios with a balanced share of RES. Again, the results from RES drought
411 modelling rely more on the precision of the wind power curve and PV panel
412 models than on the specific locations of RES farms. Atlite’s superior perfor-
413 mance highlights the importance of selecting validated models for assessing
414 RES drought risks. This careful model selection can better quantify risks,
415 support effective planning, and avoid the potential underestimation of ca-
416 pacity needs, which is essential for ensuring energy security.

417 Looking at the 57W-43PV scenario, the analysis showed a significant im-
418 provement in the management of RES droughts due to the complementary
419 nature of wind and PV generation. Wind and PV together perform better
420 in terms of reducing drought frequency and duration than either would in-
421 dividually, largely because of the seasonal anti-correlation between the two
422 energy sources. This diversification reduces the seasonal impact on RES
423 droughts, as PV generation peaks in the summer and wind generation is
424 more consistent in winter. Ireland currently has a highly wind-dependent
425 energy system, but with ambitious targets for PV installations in the coming
426 years, the energy mix is expected to approach a balance between wind and
427 PV capacity. While this balanced approach offers a more stable and secure
428 energy supply by mitigating RES drought risks, it is important to note that
429 having similar wind and PV capacities may not optimise other aspects, such
430 as annual energy production or meeting nighttime loads. For policymakers,
431 these findings underscore the importance of meeting these capacity targets
432 to enhance energy security through diversification. Additionally, the choice

433 of model for RES drought assessment becomes increasingly critical as more
434 renewable capacity is integrated into the system.

435 Future work is planned to extend the current analysis. First, climate
436 projection data will be integrated with different energy scenarios, incorpo-
437 rating the addition of offshore wind, to better understand how climate change
438 might affect RES droughts. Second, expanding the geographic domain of the
439 study to include the rest of Europe would provide a more comprehensive un-
440 derstanding of RES droughts in an interconnected energy grid. This would
441 require extensive verification across other European countries, making it a
442 more complex but highly relevant challenge.

443 Data Availability

444 The ERA5 data can be obtained from the Climate Data Store (<https://doi.org/10.24381/cds.adbb2d47>). The C3S-E dataset is also available
445 from the Climate Data Store (<https://doi.org/10.24381/cds.4bd77450>).
446 Information on wind and PV farms in Ireland can be obtained from the
447 EirGrid website ([https://www.eirgrid.ie/grid/system-and-renewable](https://www.eirgrid.ie/grid/system-and-renewable-data-reports)
448 [-data-reports](https://www.eirgrid.ie/grid/system-and-renewable-data-reports)). The Atlite model used in this study is open-source and can
449 be found on GitHub (<https://github.com/pypsa/atlite>). The data and
450 code required to reproduce the analysis in this article will be made available
451 upon acceptance of the manuscript in a public GitHub repository.
452

453 Acknowledgments

454 The research conducted in this publication was funded by Science Foun-
455 dation Ireland and co-funding partners under grant number 21/SPP/3756
456 through the NexSys Strategic Partnership Programme.

457 References

- 458 [1] EuroStat, Renewable Energy Statistics, 2023. URL: [https://ec.europa.eu/eurostat/statistics-explained/index.php?title=Renewable](https://ec.europa.eu/eurostat/statistics-explained/index.php?title=Renewable_energy_statistics)
459 [energy_statistics](https://ec.europa.eu/eurostat/statistics-explained/index.php?title=Renewable_energy_statistics), Accessed: 2024-11-06.
460
- 461 [2] H. C. Bloomfield, D. J. Brayshaw, L. C. Shaffrey, P. J. Coker, H. E.
462 Thornton, Quantifying the increasing sensitivity of power systems to
463 climate variability, *Environmental Research Letters* 11 (2016) 124025.
464 doi:10.1088/1748-9326/11/12/124025.

- 465 [3] H. C. Bloomfield, D. J. Brayshaw, A. Troccoli, C. M. Goodess, M. De Fe-
466 lice, L. Dubus, P. E. Bett, Y.-M. Saint-Drenan, Quantifying the
467 sensitivity of european power systems to energy scenarios and cli-
468 mate change projections, *Renewable Energy* 164 (2021) 1062–1075.
469 doi:10.1016/j.renene.2020.09.125.
- 470 [4] K. van der Wiel, L. P. Stoop, B. R. H. Van Zuijlen, R. Blackport, M. A.
471 Van den Broek, F. M. Selten, Meteorological conditions leading to ex-
472 treme low variable renewable energy production and extreme high en-
473 ergy shortfall, *Renewable and Sustainable Energy Reviews* 111 (2019)
474 261–275. doi:10.1016/j.rser.2019.04.065.
- 475 [5] F. Kaspar, M. Borsche, U. Pfeifroth, J. Trentmann, J. Drücke, P. Becker,
476 A climatological assessment of balancing effects and shortfall risks of
477 photovoltaics and wind energy in germany and europe, *Advances in*
478 *Science and Research* 16 (2019) 119–128. doi:10.5194/asr-16-119-2
479 019.
- 480 [6] M. Ohba, Y. Kanno, D. Nohara, Climatology of dark doldrums in japan,
481 *Renewable and Sustainable Energy Reviews* 155 (2022) 111927. doi:10
482 .1016/j.rser.2021.111927.
- 483 [7] F. Mockert, C. M. Grams, T. Brown, F. Neumann, Meteorological
484 conditions during periods of low wind speed and insolation in Germany:
485 The role of weather regimes, *Meteorological Applications* 30 (2023)
486 e2141. doi:10.1002/met.2141.
- 487 [8] M. J. Mayer, B. Biró, B. Szücs, A. Aszódi, Probabilistic modeling of
488 future electricity systems with high renewable energy penetration using
489 machine learning, *Applied Energy* 336 (2023) 120801. doi:10.1016/j.
490 apenergy.2023.120801.
- 491 [9] D. Raynaud, B. Hingray, B. François, J. Creutin, Energy droughts from
492 variable renewable energy sources in European climates, *Renewable*
493 *Energy* 125 (2018) 578–589. doi:https://doi.org/10.1016/j.renene
494 .2018.02.130.
- 495 [10] K. Z. Rinaldi, J. A. Dowling, T. H. Ruggles, K. Caldeira, N. S. Lewis,
496 Wind and Solar Resource Droughts in California Highlight the Benefits
497 of Long-Term Storage and Integration with the Western Interconnect,

- 498 Environmental Science and Technology 55 (2021) 6214–6226. doi:10.1
499 021/acs.est.0c07848.
- 500 [11] A. Gangopadhyay, A. K. Seshadri, N. J. Sparks, R. Toumi, The role
501 of wind-solar hybrid plants in mitigating renewable energy-droughts,
502 Renewable Energy 194 (2022) 926–937. doi:10.1016/j.renene.2022.
503 05.122.
- 504 [12] S. Allen, N. Otero, Standardised indices to monitor energy droughts,
505 Renewable Energy 217 (2023) 119206. doi:10.1016/j.renene.2023.11
506 9206.
- 507 [13] J. Kapica, J. Jurasz, F. A. Canales, H. Bloomfield, M. Guezgouz,
508 M. De Felice, Z. Kobus, The potential impact of climate change on
509 european renewable energy droughts, Renewable and Sustainable En-
510 ergy Reviews 189 (2024) 114011. doi:10.1016/j.rser.2023.114011.
- 511 [14] C. Bracken, N. Voisin, C. D. Burleyson, A. M. Campbell, Z. J. Hou,
512 D. Broman, Standardized benchmark of historical compound wind and
513 solar energy droughts across the Continental United States, Renewable
514 Energy 220 (2024) 119550. doi:https://doi.org/10.1016/j.renene
515 .2023.119550.
- 516 [15] H. Hersbach, B. Bell, P. Berrisford, S. Hirahara, A. Horányi, J. Muñoz-
517 Sabater, J. Nicolas, C. Peubey, R. Radu, D. Schepers, et al., The ERA5
518 global reanalysis, Quarterly Journal of the Royal Meteorological Society
519 146 (2020) 1999–2049. doi:10.1002/qj.3803.
- 520 [16] L. Dubus, Y. Saint-Drenan, A. Troccoli, M. De Felice, Y. Moreau, L. Ho-
521 Tran, C. Goodess, R. Amaro E Silva, L. Sanger, C3S Energy: A climate
522 service for the provision of power supply and demand indicators for Eu-
523 rope based on the ERA5 reanalysis and ENTSO-E data, Meteorological
524 Applications 30 (2023) e2145. doi:10.1002/met.2145.
- 525 [17] Copernicus Climate Change Service (C3S), Climate and energy indi-
526 cators for Europe from 1979 to present derived from reanalysis., 2020.
527 doi:10.24381/cds.4bd77450, accessed on 28-11-2024.
- 528 [18] F. Hofmann, J. Hampp, F. Neumann, T. Brown, J. Hörsch, Atlite: a
529 lightweight Python package for calculating renewable power potentials

- 530 and time series, *Journal of Open Source Software* 6 (2021) 3294. doi:10
531 .21105/joss.03294.
- 532 [19] J. Li, Z. Zhao, D. Xu, P. Li, Y. Liu, M. A. Mahmud, D. Chen, The
533 potential assessment of pump hydro energy storage to reduce renewable
534 curtailment and CO2 emissions in Northwest China, *Renewable Energy*
535 212 (2023) 82–96. doi:10.1016/j.renene.2023.04.132.
- 536 [20] M. Parzen, H. Abdel-Khalek, E. Fedotova, M. Mahmood, M. M. Frysztacki,
537 J. Hampp, L. Franken, L. Schumm, F. Neumann, D. Poli,
538 et al., Pypsa-earth. a new global open energy system optimization
539 model demonstrated in africa, *Applied Energy* 341 (2023) 121096.
540 doi:10.1016/j.apenergy.2023.121096.
- 541 [21] K. Ali Khan Niazi, M. Victoria, Comparative analysis of photovoltaic
542 configurations for agrivoltaic systems in europe, *Progress in Photo-*
543 *voltatics: Research and Applications* 31 (2023) 1101–1113. doi:10.1002/
544 pip.3727.
- 545 [22] EirGrid & SONI, System and Renewable Data Reports, 2023. URL:
546 [https://www.eirgrid.ie/grid/system-and-renewable-data-rep](https://www.eirgrid.ie/grid/system-and-renewable-data-reports)
547 [orts](https://www.eirgrid.ie/grid/system-and-renewable-data-reports), Accessed: 2024-11-06.
- 548 [23] P. T. Brown, D. J. Farnham, K. Caldeira, Meteorology and climatology
549 of historical weekly wind and solar power resource droughts over western
550 North America in ERA5, *SN Applied Sciences* 3 (2021) 814. doi:10.1
551 007/s42452-021-04794-z.
- 552 [24] N. Otero, O. Martius, S. Allen, H. Bloomfield, B. Schaeffli, Character-
553 izing renewable energy compound events across Europe using a logistic
554 regression-based approach, *Meteorological Applications* 29 (2022) e2089.
555 doi:10.1002/met.2089, 13.
- 556 [25] Y.-M. Saint-Drenan, L. Wald, T. Ranchin, L. Dubus, A. Troccoli, An
557 approach for the estimation of the aggregated photovoltaic power gener-
558 ated in several European countries from meteorological data, *Advances*
559 *in Science and Research* 15 (2018) 51–62. doi:10.5194/asr-15-51-201
560 8.

- 561 [26] I. Staffell, S. Pfenninger, Using bias-corrected reanalysis to simulate
562 current and future wind power output, *Energy* 114 (2016) 1224–1239.
563 doi:10.1016/j.energy.2016.08.068.
- 564 [27] Government of Ireland, Climate Action Plan 2024, Technical Report 3,
565 Department of the Environment, Climate and Communications, 2023.
566 URL: [https://www.gov.ie/pdf/?file=https://assets.gov.ie/](https://www.gov.ie/pdf/?file=https://assets.gov.ie/284675/70922dc5-1480-4c2e-830e-295afd0b5356.pdf)
567 [284675/70922dc5-1480-4c2e-830e-295afd0b5356.pdf](https://www.gov.ie/pdf/?file=https://assets.gov.ie/284675/70922dc5-1480-4c2e-830e-295afd0b5356.pdf), Accessed:
568 2024-11-06.
- 569 [28] Sustainable Energy Authority Ireland, National Energy Projections
570 2024, Technical Report, Sustainability Energy Authority of Ireland,
571 2024. URL: [https://www.seai.ie/news-and-events/news/energ](https://www.seai.ie/news-and-events/news/energy-projections-report)
572 [y-projections-report](https://www.seai.ie/news-and-events/news/energy-projections-report), Accessed: 2024-11-06.
- 573 [29] H. G. Beyer, G. Heilscher, S. Bofinger, A robust model for the mpp
574 performance of different types of pv-modules applied for the performance
575 check of grid connected systems, *Eurosun* (2004) 8.